

Flux Variations of Fast Radio Bursts and Their Persistent Radio Sources: Evidence for a Shared Progenitor

XINMING LI ^{1,2} CHEN-HUI NIU ^{1,2} JIA-HENG ZHANG ^{1,2} DI LI ^{3,4} BING ZHANG ^{5,6,7,8} YUAN-PEI YANG ⁹
PEI WANG ⁴ JUNSHUO ZHANG ^{4,10} YONGKUN ZHANG ⁴ YE LI ^{11,12} JIARUI NIU ⁴ XIAOPING ZHENG ^{1,2}
YUNWEI YU ^{1,2} YI FENG ^{13,14} FAYIN WANG ^{15,16} YUHAO ZHU ^{4,10} AMING CHEN ^{1,2} ZE-XIN DU ^{1,2}
JIAN LI ^{17,12} WEIHONG LI ^{1,2} CHENCHEN MIAO ^{18,19} WEIYANG WANG ¹⁰ GUANG-LEI WU ^{1,2}
AI YUAN YANG ^{4,20} JUMEI YAO ²¹ AND RU-SHUANG ZHAO ²²

¹Laboratory for Compact Object Astrophysics and AstroSpace Technology, Central China Normal University, Wuhan 430079, China

²Institute of Astrophysics, Central China Normal University, Wuhan 430079, China

³Department of Astronomy, Tsinghua University, Beijing 100084, China

⁴National Astronomical Observatories, Chinese Academy of Sciences, Beijing 100101, China

⁵The Hong Kong Institute for Astronomy and Astrophysics, The University of Hong Kong, Pokfulam, Hong Kong, P. R. China

⁶Department of Physics, The University of Hong Kong, Pokfulam, Hong Kong, P. R. China

⁷Nevada Center for Astrophysics, University of Nevada, Las Vegas, USA

⁸Department of Physics and Astronomy, University of Nevada, Las Vegas, USA

⁹South-Western Institute for Astronomy Research, Yunnan Key Laboratory of Survey Science, Yunnan University, Kunming, P. R. China

¹⁰School of Astronomy and Space Science, University of Chinese Academy of Sciences, Beijing 100049, China

¹¹Purple Mountain Observatory, Chinese Academy of Sciences, Nanjing, P. R. China

¹²School of Astronomy and Space Sciences, University of Science and Technology of China, Hefei, P. R. China

¹³Research Center for Astronomical Computing, Zhejiang Laboratory, Hangzhou, P. R. China

¹⁴Institute for Astronomy, School of Physics, Zhejiang University, Hangzhou, P. R. China

¹⁵School of Astronomy and Space Science, Nanjing University, Nanjing 210093, China

¹⁶Key Laboratory of Modern Astronomy and Astrophysics (Nanjing University), Ministry of Education, Nanjing 210093, China

¹⁷Department of Astronomy, University of Science and Technology of China, Hefei, China

¹⁸Department of Astronomy, College of Physics and Electronic Engineering, Qilu Normal University, Jinan 250200, China

¹⁹Shandong Key Laboratory of Space Environment and Exploration Technology, No. 180, Wenhua West Road, Weihai City, Shandong Province 264209, People's Republic of China

²⁰Key Laboratory of Radio Astronomy and Technology, Chinese Academy of Sciences, A20 Datun Road, Chaoyang District, Beijing, 100101, P. R. China

²¹Xinjiang Astronomical Observatory, Chinese Academy of Sciences, Urumqi 830011, China

²²Guizhou Normal University, Guiyang 550001, China

ABSTRACT

Fast radio bursts (FRBs) are millisecond-duration extragalactic radio transients, some of which are associated with compact persistent radio sources (PRSSs), hinting at a physical connection. While several models have been proposed to explain PRSSs and their connection to FRBs, direct observational tests remain limited. Here, we report for the first time a correlated trend between the long-term variation of the PRS flux density and the burst energetics of FRB 20190520B and FRB 20240114A, suggesting that both the PRS and FRB activity may be powered by a shared energy reservoir. We further examine additional repeaters with compact PRSSs and find no clear correlation between PRS luminosity and burst activity, likely due to the limited observations. These results are consistent with scenarios in which both the PRS and FRB activity may be powered by a common energy reservoir, such as the magnetic or rotational energy of a magnetar.

Keywords: Fast radio burst, Persistent radio source, FRB 20190520B, FRB 20240114A

1. INTRODUCTION

Fast radio bursts (FRBs) are millisecond-duration radio transients with extremely high brightness tem-

peratures at extragalactic distances, whose central engine and emission physics remain debated (D. R. Lorimer et al. (2007); CHIME/FRB Collaboration et al. (2021); E. Petroff et al. (2022); B. Zhang (2023)). As the detected sample has grown, a subset of FRBs has been found to repeat (L. G. Spitler et al. (2016)). The discovery of repeating activity is pivotal, enabling precise localizations and systematic follow-up across multiple epochs and frequencies (S. Chatterjee et al. (2017); B. Marcote et al. (2017)).

For several well-localized repeating FRBs, compact, non-thermal persistent radio sources (PRSs) have been found in spatial coincidence with the FRB positions; these sources are unresolved on milliarcsecond scales and exhibit GHz-band power-law spectra with radio luminosities up to $L_\nu \sim 10^{27-29} \text{ erg s}^{-1} \text{ Hz}^{-1}$. Typical cases include two PRSs spatially associated with FRB 20121102A (S. Chatterjee et al. (2017); B. Marcote et al. (2017)) and FRB 20190520B (C.-H. Niu et al. (2022)), along with lower-luminosity PRSs associated with FRB 20201124A (V. Ravi et al. (2022); G. Bruni et al. (2024)), FRB 20240114A (G. Bruni et al. (2025); X. Zhang et al. (2025)), and FRB 20190417A (A. M. Moroianu et al. (2025)). At the same time, many repeating FRBs show no detectable persistent radio sources (PRS), even at deep observational limits. This indicates that bright PRSs may not be a universal feature of such repeaters, or that their sources may lie at different evolutionary stages.

Whether PRSs are physically linked to FRBs remains a central question. An empirical correlation between PRS luminosity and $|\text{RM}|$ has been proposed (Y.-P. Yang et al. (2020)). The most luminous PRS systems tend to show extreme rotation measures ($|\text{RM}| \sim 10^{4-5} \text{ rad m}^{-2}$), while lower-luminosity PRS candidates exhibit milder RMs ($\sim 10^2 \text{ rad m}^{-2}$). On intra-source timescales, short-term correlations between PRS flux variations and FRB burst energy are often insignificant. Some sources show modulation beyond what is expected from pure refractive interstellar scintillation (RISS), indicating intrinsic PRS variability or a complex scattering environment (e.g., S. Chatterjee et al. (2017); X. Zhang et al. (2025)).

Theoretically, a young magnetar is one of the most widely discussed explanations for FRBs and their associated persistent radio emission. Even prior to the discovery of the first persistent radio source, it was proposed that the relativistic outflow from a young magnetar could inflate a magnetar wind nebula (MWN), producing long-lived synchrotron emission (Y.-P. Yang et al. (2016)). In this framework, the relativistic wind launched by the magnetar inflates a nebula that pow-

ers the persistent radio emission through synchrotron radiation from relativistic electrons, naturally linking high $|\text{RM}|$, large host-galaxy dispersion measures, and a dense, turbulent local environment (B. D. Metzger et al. (2017); B. Margalit & B. D. Metzger (2018)). This scenario is closely related to the earlier pulsar wind nebula (PWN) paradigm and was later applied to explain the compact PRS associated with FRB 20121102. Interaction between the MWN and the surrounding supernova remnant can naturally produce a composite system in which the nebula powers the persistent radio emission while the expanding remnant dominates the propagation effects, such as large and evolving RM and DM (Z. Y. Zhao & F. Y. Wang (2021)). Additionally, alternative classes of models invoke accretion-powered compact objects. In the ‘‘hypernebula’’ scenario, powerful outflows launched by a hyper-accreting compact object inflate a compact synchrotron nebula and can account for the observed PRS luminosity and large Faraday rotation (N. Sridhar & B. D. Metzger 2022). Other works instead associate the PRS with radio emission from low-luminosity AGNs or massive/intermediate-mass black holes in dense galactic environments (Y. Dong et al. 2024). These models suggest that PRSs may be powered by distinct compact objects or energy sources, requiring future observations to determine the dominant mechanisms behind these emissions.

Among repeating FRBs associated with PRSs, FRB 20190520B and FRB 20240114A stand out for their persistent activity and exceptionally high burst rates, respectively. FRB 20190520B sustained multi-year activity and extreme, rapidly evolving propagation properties. Its DM is exceptionally large and declining steadily at $\sim 10 \text{ pc cm}^{-3} \text{ yr}^{-1}$ (C.-H. Niu et al. (2026)). Additionally, its RM reaches extreme absolute values and undergoes dramatic temporal evolution, including sign reversals. Highly variable millisecond-scale scattering further indicates a dynamic, inhomogeneous local plasma environment (S. K. Ocker et al. (2023)). These properties suggest a young magnetar embedded in a dense and highly magnetized environment, possibly associated with an expanding supernova remnant (F. Y. Wang et al. (2025)), where the compact PRS naturally arises from a MWN. Furthermore, its predominantly narrow-band, intrinsically generated bursts point to a magnetospheric origin (Y. Zhu et al. (2024); J. Heng Zhang et al. (2025)). FRB 20240114A was first reported by CHIME (K. Shin & CHIME/FRB Collaboration (2024)). Subsequent follow-up observations with FAST revealed an exceptionally high burst rate, with more than 11,000 bursts detected over a monitoring window of approximately 214 days, making it one of the most burst-active

FRB sources identified to date (J.-S. Zhang et al. (2025)). Despite this intense bursting activity, the RM has not exhibited significant temporal variation over the limited epochs currently available (J.-T. Xie et al. (2025)).

Despite these advances, the connection between PRS properties and FRB activity remains poorly understood. Assuming a co-source magnetar model, we expect these components to be physically coupled within the system. Specifically, progenitor energy releases and FRB bursts may share a common physical origin, or energy from the FRBs could be deposited into the surrounding nebula, driving contemporaneous or delayed variations in the PRS flux density. These expectations motivate our systematic investigation of the correlation between PRS emission and FRB energy output.

In this paper, we investigate the statistical and physical connections between repeating FRBs and their associated PRSs. Section 2 describes the compiled dataset, introduces a proxy for the central engine’s daily energy output, and outlines the methods used to analyze its correlation with PRS emission. Section 3 presents the observational results and the quantitative outcomes of the correlation analysis. Section 4 discusses the physical implications of these findings, including the intrinsic origin of PRS variability and the possibility of a shared energy reservoir that powers both FRB bursts and PRS emission. Finally, Section 5 summarizes our main conclusions.

2. DATA AND ANALYSIS METHODS

2.1. Data

We compile data for five FRB–PRS systems that have been reported to host compact persistent radio sources or persistent radio counterparts. For each system, we compile all available PRS flux-density measurements together with the FRB burst data obtained during the corresponding periods of PRS monitoring, focusing on observational campaigns that span extended time intervals. The burst sample is restricted to L-band observations, where the observational coverage is the most extensive for these repeaters, enabling a more uniform and statistically robust characterisation of their burst activity. The references for all PRS and burst data used in this work are summarised in Table 1.

2.2. A daily energy–output proxy

To quantify the energy that each repeater injects into its surrounding environment on observable timescales, we construct a simple activity indicator based on the detected bursts. For each observing day, we calculate the total fluence of all detected bursts normalized by the effective observing time. This yields a daily en-

ergy–output proxy

$$P_{\text{day}} \equiv \frac{\sum_{i=1}^N F_i}{T_{\text{obs}}}, \quad (1)$$

where N is the number of bursts detected on that observing day, F_i denotes the fluence of the i -th burst, and T_{obs} is the total effective observing time of that day. Here, P measures the fluence accumulated per unit observing time and thus serves as a proxy for the daily burst energy output (or activity level) during a given observing epoch.

2.3. Correlation analysis method

2.3.1. Time-window–based paired correlation analysis

In addition to the ICCF analysis, we apply a time-window–based paired correlation method to test whether the FRB activity and the PRS emission exhibit synchronous variations on finite timescales, without assuming a fixed time lag. For each PRS observation epoch, we compute the mean FRB activity proxy $\langle P \rangle$ within a symmetric time window centered on that epoch, and pair it with the corresponding PRS flux density. Correlations between the paired quantities are evaluated using both Pearson and Spearman statistics. To assess statistical significance, we perform permutation tests by randomly shuffling the window-averaged FRB activity values while keeping the PRS flux measurements fixed, and recomputing the correlation coefficients. This procedure is repeated for multiple window sizes to examine the robustness of the results across different timescales. Because the windowed pairs are not strictly independent, the permutation-based p-values are adopted as the primary measure of significance.

2.3.2. Interpolated cross-correlation function (ICCF)

Because the PRS and FRB observations are unevenly sampled and not strictly simultaneous, we employ the ICCF method (R. J. White & B. M. Peterson 1994) to investigate possible correlations between the PRS flux density and the daily energy–output proxy P_{day} .

In the ICCF analysis, correlations are evaluated by shifting one time series relative to the other and linearly interpolating it onto the sampling epochs of the second series. To mitigate possible interpolation bias, the ICCF is computed in both interpolation directions, by alternatively interpolating P_{day} to the PRS observing epochs and interpolating the PRS flux densities to the epochs of P_{day} . The final ICCF is then obtained by averaging the two resulting correlation functions.

We quantify the correlation using both the Pearson correlation coefficient, which measures linear relationships, and the Spearman rank correlation coefficient,

Table 1. L-band FRB Observations and Persistent Radio Source Flux Density Measurements for Five FRB–PRS Systems

source	Ref(Flux density)	Observation time ^a	telescope ^b	Ref(Burst rate)	Observation time	telescope
20121102A	S. Chatterjee et al. (2017)	2016.4–9 (37)	VLA(S)	D. M. Hewitt et al. (2022)	2015.11–2016.10	Arecibo
	B. Marcote et al. (2017)	2016.2–9 (6)	EVN(L,C)	D. Li et al. (2021)	2019.8–10	FAST
	L. Resmi et al. (2021)	2017.5–12 (4)	GMRT(P,L)	P. Wang et al. (2025)	2020.3–2023.4	FAST
	A. Plavin et al. (2022)	2017.2–11 (6)	EVN(L,C)			
	G. Chen et al. (2023)	2017.5–8 (7)	VLA(Ku,K)			
	L. Rhodes et al. (2023)	2019.9–2022.9 (5)	MeerKAT(L)			
	A. Y. Yang et al. (2024)	2023.5–6 (9)	VLA(L)			
	M. Bhardwaj et al. (2025)	2022.11–2023.8 (8)	GMRT(P,L)			
20190520B	C.-H. Niu et al. (2022)	2020.7–11 (14)	VLA(L,S,C)	C.-H. Niu et al. (2022)	2020.4–2020.9	FAST
	X. Zhang et al. (2023)	2021.10–11 (8)	VLA(L,S,C,X)	C.-H. Niu et al. (2026)	2020.4–2023.3	FAST
	S. Bhandari et al. (2023)	2022.2 (2)	EVN(L)	In prep. (Zhang)	2020.4–2024.12	FAST
	A. Y. Yang et al. (2024)	2023.6 (7)	VLA(S)			
	A. Balasubramanian et al. (2025)	2022.11–2024.9 (8)	GMRT(L)			
20201124A	G. Bruni et al. (2024)	2021.10–2022.3 (3)	VLA(C,Ku,K)	H. Xu et al. (2022)	2021.4–6	FAST
	-	-	-	Y.-K. Zhang et al. (2022)	2021.9–10	FAST
20240114A	G. Bruni et al. (2025)	2024.9 (2)	VLBA(C)	J.-S. Zhang et al. (2025)	2024.1–2024.8	FAST
	X. Zhang et al. (2025)	2024.2–10 (11)	VLA(L,S,C) MeerKAT(L)			
	Y. Bhusare et al. (2025)	2024.2–8 (7)	GMRT(P)			
20190417A	A. M. Moroianu et al. (2025)	2021.10–2022.8(1)	EVN(L)	Y. Feng et al. (2025)	2020.8–2022.11	FAST

^aThis column lists the time span of the PRS observations, with the number in parentheses indicating the total number of observing epochs within that interval.

^bThis column specifies the telescope and the associated observing frequency band used in the PRS observations.

which is sensitive to monotonic trends and less affected by outliers. Uncertainties are estimated using a flux-randomization bootstrap procedure (B. Peterson et al. (1998)), in which the PRS flux measurements are perturbed according to their reported uncertainties and re-sampled with replacement.

To evaluate the statistical significance of the correlation, we perform permutation tests by randomly shuffling the temporal order of one time series while keeping the other fixed. The ICCF is recomputed for each of 1000 permutations, and the empirical p -value is defined as the fraction of trials whose maximum correlation coefficient exceeds that obtained from the real data.

3. ANALYSIS AND RESULTS

3.1. FRB 20190520B

Within our sample, FRB 20190520B provides the most robust dataset. Its burst activity has been monitored exclusively with FAST over several years, thereby avoiding sensitivity differences among telescopes, and its PRS has been observed in multiple epochs since its discovery. To place all PRS flux-density measurements on a common frequency scale, we scale the reported values to 3 GHz assuming a power-law spectrum with a spectral index

of $\alpha = -0.375$ (A. Balasubramanian et al. (2025)), as shown in Figure 1.

The PRS light curve of FRB 20190520B shows noticeable variability over the observational baseline, as illustrated in Figure 1. In particular, the GMRT observations obtained around December 2022 display pronounced short-timescale fluctuations in the PRS flux density. Such enhanced variability is likely associated with transient changes in the local environment of the source, for example variations in absorption, scattering, or plasma conditions along the line of sight. These environmental effects may temporarily amplify the observed PRS flux and perturb the underlying co-evolution between the PRS emission and FRB activity.

To mitigate the influence of these transient environmental effects, we restrict our correlation analysis to the remaining observational epochs. We then construct paired samples using the time-window pairing method described above and evaluate their correlations using both Pearson and Spearman statistics. The statistical significance is assessed through 5000 permutation realizations. The results are summarized in Table 2. Across different time-window configurations, the Spearman test consistently yields statistically significant positive correlations for both sources. The Pearson statistic, however,

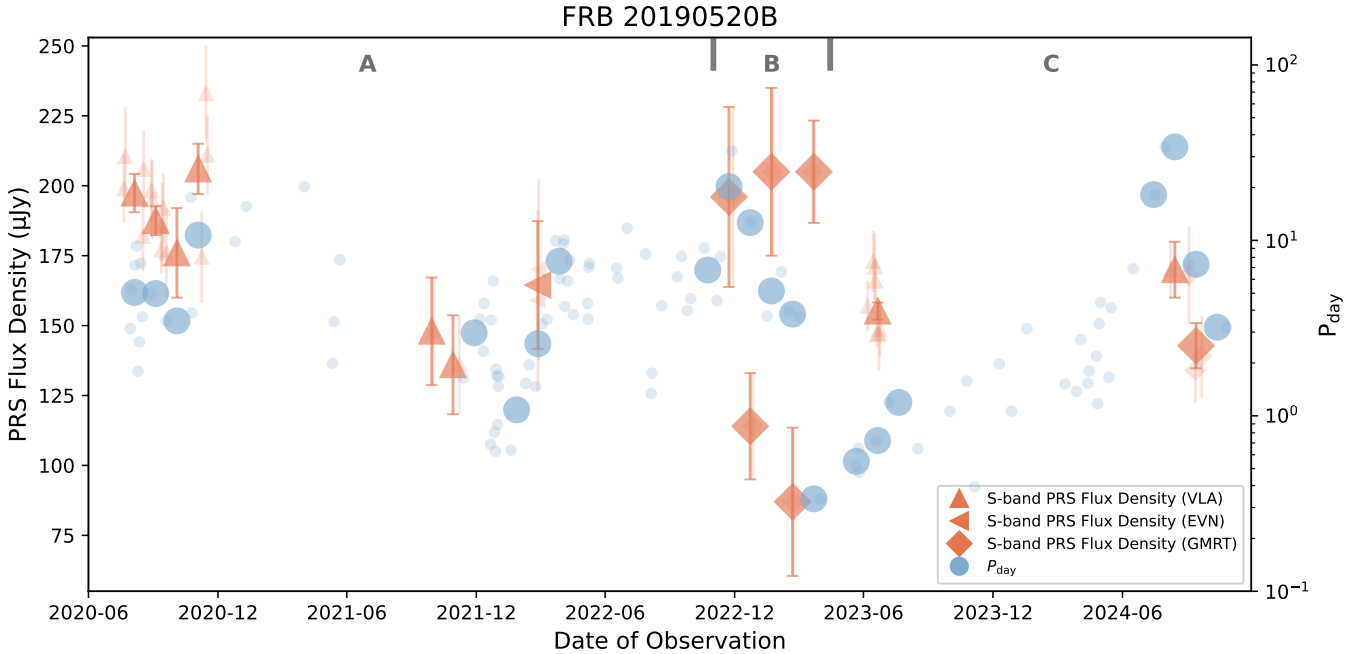


Figure 1. PRS flux density of FRB 20190520B and the corresponding daily FRB activity proxy P_{day} . The smaller orange symbols denote individual PRS flux-density measurements, which have been uniformly converted to the S band under the assumption of a power-law spectrum. The smaller blue markers represent the daily energy-output proxy P_{day} , calculated from FRB bursts detected by FAST. The detailed values of the S-band-converted PRS flux densities and the corresponding P_{day} are listed in Appendix Table 3 and Table 4. The larger orange and blue symbols indicate the binned PRS flux density and P_{day} , respectively, obtained using a 30-day binning scheme starting from the first PRS observation. In addition, the VLA observations obtained in June 2023 were analyzed in both A. Y. Yang et al. (2024) and A. Balasubramanian et al. (2025), yielding slightly different results due to differences in the data-reduction procedures. In this work, we adopt the most recent processing results presented in A. Balasubramanian et al. (2025).

shows significant correlations for FRB 20240114A across all tested windows and for FRB 20190520B at the ± 5 d and ± 7.5 d windows, but becomes insignificant for FRB 20190520B at the ± 10 d window. This behavior is expected because the Pearson coefficient measures strictly linear relationships and is more sensitive to scatter and outliers, whereas the Spearman rank statistic captures monotonic trends and is more robust to non-Gaussian variability. These results therefore suggest that the PRS flux density and FRB activity exhibit coordinated variability on weekly to monthly timescales.

Table 2. Results of the time-window pairing method.

source	Window	Pearson r	perm- p	Spearman ρ	perm- p
0520B	± 5 d	+0.88	2.0×10^{-4}	+0.86	2.0×10^{-4}
	± 7.5 d	+0.77	4.0×10^{-4}	+0.79	6.0×10^{-4}
	± 10 d	+0.13	0.59	+0.72	8.0×10^{-4}
0114A	± 5 d	+0.78	1.3×10^{-2}	+0.84	8.0×10^{-3}
	± 7.5 d	+0.79	1.3×10^{-2}	+0.87	3.8×10^{-3}
	± 10 d	+0.82	8.4×10^{-3}	+0.95	6.0×10^{-4}

To further investigate the temporal relationship between the two quantities, we also perform an ICCF anal-

ysis. However, during the later observational stage only a few PRS measurements are available, and these points are separated from the earlier data by a substantial temporal gap. Including such sparse measurements in the ICCF calculation would require extensive interpolation and could artificially enhance the apparent correlation. We therefore restrict the ICCF analysis to the earlier observing interval where the PRS observations are relatively continuous.

Within this interval, the ICCF analysis shows that P_{day} and the PRS flux density remain positively correlated over a broad range of time lags. The correlation coefficient varies smoothly with lag and does not exhibit a sharp peak at any particular delay. In addition, the lag corresponding to the maximum correlation differs between correlation estimators, indicating that the time lag itself is not robustly constrained. Nevertheless, significance tests for the maximum correlation obtained with each estimator still indicate statistically meaningful correlations (see Appendix Figure 3).

Taken together, these results suggest the presence of a positive relationship between FRB activity and PRS emission in FRB 20190520B. Although the absence of a

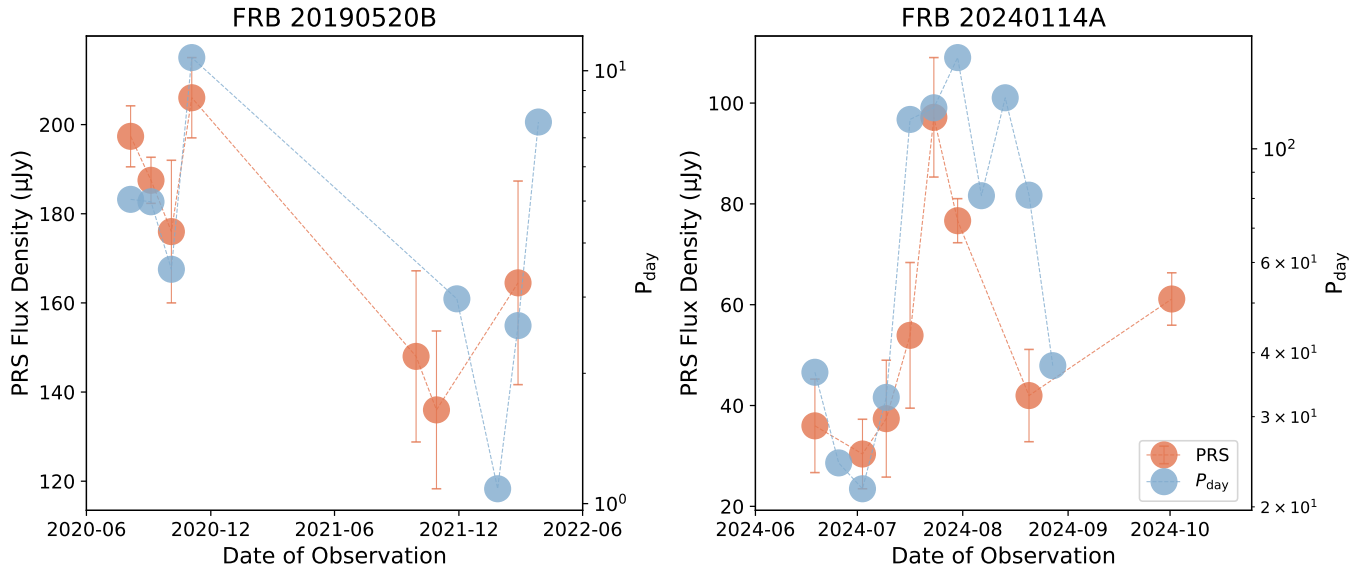


Figure 2. Co-variation of PRS Flux Density and FRB Activity in FRB 20190520B and FRB 20240114A. Both panels show binned results. A 30-day bin size (Segment A data) is adopted for FRB 20190520B, while a 7-day binning scheme is used for FRB 20240114A. Because a single bin for FRB 20240114A may contain measurements from multiple telescopes, the binned PRS data are not further distinguished by telescope symbols.

sharp correlation peak prevents a precise measurement of the time delay, the coherent variability observed on weekly to monthly timescales is consistent with a scenario in which both phenomena are driven by a common central engine. Variability on shorter timescales, however, may be influenced or partially masked by fluctuations in the local environment surrounding the source.

3.2. FRB 20240114A

For FRB 20240114A, we homogenize all burst measurements obtained at different observing frequencies by converting them to an equivalent 3 GHz fluence, assuming a spectral index of -0.34 . Based on these rescaled fluences, we derive the corresponding burst activity proxy P for each observing epoch. The resulting time series is presented in Figure 2. We first perform a binned correlation analysis between the PRS flux density and the burst activity proxy. Given the available binned data, we quantify the correlation using both Pearson and Spearman coefficients and evaluate the statistical significance through 5000 permutation realizations. This analysis reveals a clear positive correlation (Pearson $r=+0.8352$, perm- $p=1.4 \times 10^{-2}$; Spearman $\rho=+0.9286$, perm- $p=7.399 \times 10^{-3}$). To further assess the robustness of this finding, we apply the time-window-based pairing method described above. The resulting correlation coefficients and permutation-based p -values are summarized in Table 2 and likewise indicate a positive correlation. Together, these results demonstrate that, on weekly to monthly timescales, the PRS

flux density and the FRB burst energetics exhibit synchronous positive variability. A similar trend has also been mentioned in recent monitoring reports (X. Zhang & W. Yu (2026)), consistent with the correlation identified in this work.

3.3. Analysis of the Remaining FRB-PRS Systems

For FRB 20121102A, we compile PRS flux-density measurements accumulated over multiple years. However, contemporaneous FRB observations are sparse and unevenly distributed in time, which makes a robust correlation analysis over the full dataset impractical. We therefore focus on the year 2016, during which both PRS and FRB observations are relatively well sampled. We note that the PRS monitoring in 2016 still contains substantial gaps between different phases of the observing season, and such sampling discontinuities may reduce the sensitivity of correlation analyses to genuine physical associations. To mitigate this effect, we further perform an additional correlation analysis for the most densely sampled sub-interval, spanning August to October 2016. Overall, we find no statistically significant correlation at any tested time lag, either over the full 2016 April–November interval or within the August–October sub-interval. The corresponding time-series data and correlation results are presented in Appendix Figures 4, 5, and 6.

For FRB 20201124A, a statistically meaningful PRS–FRB correlation analysis is currently not feasible. The putative PRS associated with this source remains

debated in the literature, with a relatively low reported radio luminosity and several measurements not originating from an unambiguously identified compact component, implying possible contamination from diffuse host-galaxy emission. As a result, only three epochs provide reliable measurements of a compact component suitable for our analysis. In addition, the publicly available FAST burst-detection data are limited to observations in 2021 and do not temporally overlap with the existing PRS measurements. For these reasons, we do not perform a correlation analysis for FRB 20201124A; a summary of the relevant observational data is presented in the Appendix Fig.7.

4. DISCUSSION

4.1. Scintillation of the PRS Variability

Propagation of radio waves from a point source through an inhomogeneous plasma can induce interstellar scintillation, which may account for the observed variability of the PRS (M. A. Walker (1998)). The impact of scintillation on the PRS of FRB 20190520B has been previously investigated (X. Zhang et al. (2023); A. Y. Yang et al. (2024)). These works suggest that the PRS of FRB 20190520B is subject to refractive scintillation, with a transition frequency of $\nu_0 = 12.5$ GHz along its LOS. Following the formalism of M. A. Walker (1998), the scattering strength is defined as $\xi = (\nu_0/\nu)^{17/10}$, and the modulation index for refractive scintillation is given by $m_p = \xi^{-1/3}$. At an observing frequency of 3 GHz, the expected modulation index is therefore $m_p = 0.44$. From the results in this paper, the $m_{\text{obs}} = \sigma_S/\bar{S} = 0.144$ does not reach the estimated m_p . We further examine the possible contribution of refractive scintillation to the variability of the PRS associated with FRB 20240114A. The theoretically expected modulation index for this source at 3 GHz is $m_p \approx 0.484$ (X. Zhang et al. (2025)). From our measurements, we obtain an observed modulation index of $m_{\text{obs}} = \sigma_S/\bar{S} = 0.356$, which does not reach the predicted scintillation value. Therefore, similar to the case of FRB 20190520B, the flux variability of the PRSs in both sources is more likely intrinsic in origin and may be physically connected to the same progenitor responsible for the FRB activity.

4.2. PRS luminosity and FRB Energetics share a common Energy reservoir

On monthly timescales, the PRS luminosity evolution shows a statistically significant positive correlation with the contemporaneous FRB burst energetics (Section 3.1 and 3.2). This correlation suggests a shared energy reservoir between PRS and bursts. Within the magne-

tar central engine paradigm, the PRS may be powered by synchrotron emission from relativistic electrons (Q.-C. Li et al. (2020)), while the energy of FRBs is drawn from the same magnetic or rotational energy supply (B. Andersen et al. (2020); C. D. Bochenek et al. (2020)).

The bursts exhibit stochastic behavior, reflecting the sudden release of energy from the underlying reservoir. In contrast, the PRS, sustained by continuous injection of relativistic electrons from the magnetar, remains persistently observable. During active burst phases, the injection rate of relativistic electrons into the surrounding nebula may be temporarily enhanced, leading to an increase in PRS luminosity. If the injection spectrum hardens or the acceleration efficiency rises during these active phases, the resulting increase in synchrotron emissivity can manifest as an upturn in PRS luminosity.

The other repeating FRBs with persistent radio sources have generally not shown a clear correlation between PRS luminosity and burst activity, likely because their burst-active windows are limited or sparsely sampled, restricting such analyses. FRB 20190520B is unique in providing both a PRS and sufficiently intensive burst monitoring to reveal a tentative connection between central engine activity and nebular emission. Similarly, FRB 20240114A also exhibits synchronous variability between the PRS luminosity and burst energetics. Although the overall monitoring duration is relatively short, the temporal overlap between PRS observations and burst activity measurements is comparatively high, enabling a meaningful correlation analysis. By contrast, FRB 121102 demonstrates that a persistent PRS can remain detectable even during quiescent burst phases, indicating that while PRS luminosity traces the cumulative energy injection from the central engine, burst production depends on more transient or stochastic processes. These comparisons highlight young or actively evolving systems such as FRB 20190520B and possibly FRB 20240114A as valuable laboratories for studying the interplay between PRS properties and FRB energetics.

5. CONCLUSION

In this work, we systematically investigate several repeating FRB systems associated with PRSs. We find that for both FRB 20190520B and FRB 20240114A, the PRS flux density is positively correlated with the contemporaneous FRB burst-energy proxy on weekly to monthly timescales, with statistical significance supported by permutation-based tests. In contrast, other repeaters known to host PRSs have not yet shown compelling evidence for such a connection, likely due to limited burst monitoring, sparse temporal sampling, or

burst activity confined to restricted active windows, all of which reduce the sensitivity of correlation analyses.

Our results suggest that the variability of PRS emission and FRB burst activity may be linked to a common central-engine energy reservoir, while being regulated by different physical processes. In this picture, the persistent radio emission traces the cumulative injection of relativistic particles into the surrounding nebula, whereas FRB bursts correspond to intermittent and impulsive energy-release events drawing from the same underlying energy supply.

We further find that the observed modulation indices of the PRSs are significantly lower than the theoretical expectations from refractive interstellar scintillation, indicating that the measured PRS variability cannot be explained by scintillation alone and likely contains a substantial intrinsic component.

Taken together, these results support a scenario in which the central engine of repeating FRBs continuously powers a surrounding synchrotron-emitting nebula while episodically producing FRB bursts. Continued long-term, multi-epoch monitoring of both burst energetics and PRS evolution will therefore be essential for clarifying the dynamical interplay between the central engine, the surrounding nebula, and the local environment.

ACKNOWLEDGMENTS

We thank the FAST data center operations team for scheduling the follow-up observations and data acquisition. This work was supported by the National Natural Science Foundation of China (NSFC; Grant Nos. 11988101, 12203069 and 12503055). C.-H. Niu also acknowledges support from the Basic Research Project of Central China Normal University, the Hubei QB Project, the CAS Youth Interdisciplinary Team and the Foundation of Guizhou Provincial Education Department (Grant No. KY(2023)059). J. R. Niu is supported by the Postdoctoral Fellowship Program of CPSF under Grant Number GZB20250737. Ju-Mei Yao was supported by the National Science Foundation of Xinjiang Uygur Autonomous Region (2022D01D85), the Major Science and Technology Program of Xinjiang Uygur Autonomous Region (2022A03013-2), and the CAS Project for Young Scientists in Basic Research (YSBR-063), the Tianshan talents program (2023TSYCTD0013), and the Chinese Academy of Sciences (CAS) "Light of West China" Program (No. xzbz-gzsys-202410 and No. 2022-XBQNXZ-015).

REFERENCES

- Andersen, B., Bandura, K., Bhardwaj, M., et al. 2020, *Nature*, 587, 54–58, doi: [10.1038/s41586-020-2863-y](https://doi.org/10.1038/s41586-020-2863-y)
- Balasubramanian, A., Bhardwaj, M., & Tendulkar, S. P. 2025, *The Astrophysical Journal*, 995, 51, doi: [10.3847/1538-4357/ae1cc4](https://doi.org/10.3847/1538-4357/ae1cc4)
- Bhandari, S., Marcote, B., Sridhar, N., et al. 2023, *ApJL*, 958, L19, doi: [10.3847/2041-8213/ad083f](https://doi.org/10.3847/2041-8213/ad083f)
- Bhardwaj, M., Balasubramanian, A., Kaushal, Y., & Tendulkar, S. P. 2025, Constraining the Origin of FRB 20121102A’s Persistent Radio Source with Long-Term Radio Observations, <https://arxiv.org/abs/2506.23861>
- Bhusare, Y., Maan, Y., & Kumar, A. 2025, Low-frequency Probes of the Persistent Radio Sources associated with Repeating FRBs, <https://arxiv.org/abs/2412.13121>
- Bochenek, C. D., Ravi, V., Belov, K. V., et al. 2020, *Nature*, 587, 59–62, doi: [10.1038/s41586-020-2872-x](https://doi.org/10.1038/s41586-020-2872-x)
- Braga, C. A., Cruces, M., Cassanelli, T., et al. 2025, *A&A*, 693, A40, doi: [10.1051/0004-6361/202451905](https://doi.org/10.1051/0004-6361/202451905)
- Bruni, G., Piro, L., Yang, Y.-P., et al. 2024, *Nature*, 632, 1014, doi: [10.1038/s41586-024-07782-6](https://doi.org/10.1038/s41586-024-07782-6)
- Bruni, G., Piro, L., Yang, Y.-P., et al. 2025, *A&A*, 695, L12, doi: [10.1051/0004-6361/202453233](https://doi.org/10.1051/0004-6361/202453233)
- Chatterjee, S., Law, C. J., Wharton, R. S., et al. 2017, *Nature*, 541, 58, doi: [10.1038/nature20797](https://doi.org/10.1038/nature20797)
- Chen, G., Ravi, V., & Hallinan, G. W. 2023, *ApJ*, 958, 185, doi: [10.3847/1538-4357/ad02f3](https://doi.org/10.3847/1538-4357/ad02f3)
- CHIME/FRB Collaboration, Amiri, M., Andersen, B. C., et al. 2021, *ApJS*, 257, 59, doi: [10.3847/1538-4365/ac33ab](https://doi.org/10.3847/1538-4365/ac33ab)
- Dong, Y., Eftekhari, T., Fong, W., et al. 2024, *ApJ*, 973, 133, doi: [10.3847/1538-4357/ad6568](https://doi.org/10.3847/1538-4357/ad6568)
- Espinoza-Dupouy, M. C., Cruces, M., Cassanelli, T., et al. 2026, Chromatic activity window of periodic fast radio bursts: FRB 20121102A and FRB 20180916B, <https://arxiv.org/abs/2507.04609>
- Feng, Y., Zhang, Y.-K., Xie, J., et al. 2025, *Science China Physics, Mechanics, and Astronomy*, 68, 289511, doi: [10.1007/s11433-024-2668-5](https://doi.org/10.1007/s11433-024-2668-5)
- heng Zhang, J., Niu, C.-H., hao Zhu, Y., et al. 2025, Statistical and Temporal Analysis of Multi-component Burst-clusters from the Repeating FRB 20190520B, <https://arxiv.org/abs/2512.03591>
- Hewitt, D. M., Snelders, M. P., Hessels, J. W. T., et al. 2022, *MNRAS*, 515, 3577, doi: [10.1093/mnras/stac1960](https://doi.org/10.1093/mnras/stac1960)

- Li, D., Wang, P., Zhu, W. W., et al. 2021, *Nature*, 598, 267, doi: [10.1038/s41586-021-03878-5](https://doi.org/10.1038/s41586-021-03878-5)
- Li, Q.-C., Yang, Y.-P., & Dai, Z.-G. 2020, *The Astrophysical Journal*, 896, 71, doi: [10.3847/1538-4357/ab8db8](https://doi.org/10.3847/1538-4357/ab8db8)
- Lorimer, D. R., Bailes, M., McLaughlin, M. A., Narkevic, D. J., & Crawford, F. 2007, *Science*, 318, 777, doi: [10.1126/science.1147532](https://doi.org/10.1126/science.1147532)
- Marcote, B., Paragi, Z., Hessels, J. W. T., et al. 2017, *ApJL*, 834, L8, doi: [10.3847/2041-8213/834/2/L8](https://doi.org/10.3847/2041-8213/834/2/L8)
- Margalit, B., & Metzger, B. D. 2018, *ApJL*, 868, L4, doi: [10.3847/2041-8213/aaedad](https://doi.org/10.3847/2041-8213/aaedad)
- Metzger, B. D., Berger, E., & Margalit, B. 2017, *ApJ*, 841, 14, doi: [10.3847/1538-4357/aa633d](https://doi.org/10.3847/1538-4357/aa633d)
- Moroianu, A. M., Bhandari, S., Drout, M. R., et al. 2025, arXiv e-prints, arXiv:2509.05174, doi: [10.48550/arXiv.2509.05174](https://doi.org/10.48550/arXiv.2509.05174)
- Niu, C.-H., Aggarwal, K., Li, D., et al. 2022, *Nature*, 606, 873, doi: [10.1038/s41586-022-04755-5](https://doi.org/10.1038/s41586-022-04755-5)
- Niu, C.-H., Li, D., Yang, Y.-P., et al. 2026, *Science Bulletin*, 71, 76, doi: <https://doi.org/10.1016/j.scib.2025.11.023>
- Ocker, S. K., Cordes, J. M., Chatterjee, S., et al. 2023, *MNRAS*, 519, 821, doi: [10.1093/mnras/stac3547](https://doi.org/10.1093/mnras/stac3547)
- Peterson, B., Wanders, I., Horne, K., et al. 1998, *Publications of the Astronomical Society of the Pacific*, 110, 660–670, doi: [10.1086/316177](https://doi.org/10.1086/316177)
- Petroff, E., Hessels, J. W. T., & Lorimer, D. R. 2022, *A&A Rv*, 30, 2, doi: [10.1007/s00159-022-00139-w](https://doi.org/10.1007/s00159-022-00139-w)
- Plavin, A., Paragi, Z., Marcote, B., et al. 2022, *MNRAS*, 511, 6033, doi: [10.1093/mnras/stac500](https://doi.org/10.1093/mnras/stac500)
- Ravi, V., Law, C. J., Li, D., et al. 2022, *MNRAS*, 513, 982, doi: [10.1093/mnras/stac465](https://doi.org/10.1093/mnras/stac465)
- Resmi, L., Vink, J., & Ishwara-Chandra, C. H. 2021, *A&A*, 655, A102, doi: [10.1051/0004-6361/202039771](https://doi.org/10.1051/0004-6361/202039771)
- Rhodes, L., Caleb, M., Stappers, B. W., et al. 2023, FRB 20121102A: images of the bursts and the varying radio counterpart, <https://arxiv.org/abs/2308.04298>
- Shin, K., & CHIME/FRB Collaboration. 2024, *The Astronomer's Telegram*, 16420, 1
- Spitler, L. G., Scholz, P., Hessels, J. W. T., et al. 2016, *Nature*, 531, 202, doi: [10.1038/nature17168](https://doi.org/10.1038/nature17168)
- Sridhar, N., & Metzger, B. D. 2022, *ApJ*, 937, 5, doi: [10.3847/1538-4357/ac8a4a](https://doi.org/10.3847/1538-4357/ac8a4a)
- Walker, M. A. 1998, *MNRAS*, 294, 307, doi: [10.1046/j.1365-8711.1998.01238.x](https://doi.org/10.1046/j.1365-8711.1998.01238.x)
- Wang, F. Y., Lan, H. T., Zhao, Z. Y., et al. 2025, arXiv e-prints, arXiv:2512.07140, <https://arxiv.org/abs/2512.07140>
- Wang, P., Zhang, J. S., Yang, Y. P., et al. 2025, arXiv e-prints, arXiv:2507.15790, doi: [10.48550/arXiv.2507.15790](https://doi.org/10.48550/arXiv.2507.15790)
- White, R. J., & Peterson, B. M. 1994, *PASP*, 106, 879, doi: [10.1086/133456](https://doi.org/10.1086/133456)
- Xie, J.-T., Feng, Y., Li, D., et al. 2025, Polarization Characteristics of the Hyperactive FRB 20240114A, <https://arxiv.org/abs/2410.10172>
- Xu, H., Niu, J. R., Chen, P., et al. 2022, *Nature*, 609, 685, doi: [10.1038/s41586-022-05071-8](https://doi.org/10.1038/s41586-022-05071-8)
- Yang, A. Y., Feng, Y., Tsai, C.-W., et al. 2024, *ApJ*, 976, 165, doi: [10.3847/1538-4357/ad7d02](https://doi.org/10.3847/1538-4357/ad7d02)
- Yang, Y.-P., Li, Q.-C., & Zhang, B. 2020, *ApJ*, 895, 7, doi: [10.3847/1538-4357/ab88ab](https://doi.org/10.3847/1538-4357/ab88ab)
- Yang, Y.-P., Zhang, B., & Dai, Z.-G. 2016, *ApJL*, 819, L12, doi: [10.3847/2041-8205/819/1/L12](https://doi.org/10.3847/2041-8205/819/1/L12)
- Zhang, B. 2023, *Rev. Mod. Phys.*, 95, 035005, doi: [10.1103/RevModPhys.95.035005](https://doi.org/10.1103/RevModPhys.95.035005)
- Zhang, J.-S., Wang, T.-C., Wang, P., et al. 2025, arXiv e-prints, arXiv:2507.14707, doi: [10.48550/arXiv.2507.14707](https://doi.org/10.48550/arXiv.2507.14707)
- Zhang, X., & Yu, W. 2026, *The Astronomer's Telegram*, 17711, 1, <https://www.astronomerstelegram.org/?read=17711>
- Zhang, X., Yu, W., Yan, Z., Xing, Y., & Zhang, B. 2025, arXiv e-prints, arXiv:2501.14247, doi: [10.48550/arXiv.2501.14247](https://doi.org/10.48550/arXiv.2501.14247)
- Zhang, X., Yu, W., Law, C., et al. 2023, *ApJ*, 959, 89, doi: [10.3847/1538-4357/ad0545](https://doi.org/10.3847/1538-4357/ad0545)
- Zhang, Y.-K., Wang, P., Feng, Y., et al. 2022, *Research in Astronomy and Astrophysics*, 22, 124002, doi: [10.1088/1674-4527/ac98f7](https://doi.org/10.1088/1674-4527/ac98f7)
- Zhao, Z. Y., & Wang, F. Y. 2021, *ApJL*, 923, L17, doi: [10.3847/2041-8213/ac3f2f](https://doi.org/10.3847/2041-8213/ac3f2f)
- Zhu, Y., Niu, C., Dai, S., et al. 2024, *Chinese Physics Letters*, 41, 109501, doi: [10.1088/0256-307X/41/10/109501](https://doi.org/10.1088/0256-307X/41/10/109501)

APPENDIX

Table 3. P_{day} Data of FRB 20190520B

Date	P_{day}^a	Date	P_{day}	Date	P_{day}	Date	P_{day}
2020-07-21	0.5122	2021-12-11	2.335	2022-05-09	7.034	2023-07-07	1.192
2020-05-22	1.448	2021-12-12	4.365	2022-05-10	7.402	2023-08-17	0.6488
2020-07-30	3.14	2021-12-21	0.6887	2022-06-17	6.951	2023-08-26	-
2020-07-31	5.205	2021-12-22	3.516	2022-06-19	6.089	2023-09-17	-
2020-08-06	7.212	2021-12-25	5.867	2022-07-02	11.73	2023-10-01	1.064
2020-08-08	9.273	2021-12-27	0.8086	2022-07-28	8.366	2023-10-25	1.578
2020-08-10	1.794	2021-12-28	0.6266	2022-08-05	1.337	2023-11-05	0.3934
2020-08-12	2.639	2021-12-29	1.847	2022-08-06	1.75	2023-11-06	-
2020-08-14	7.426	2021-12-30	1.689	2022-08-20	4.235	2023-11-12	-
2020-08-16	3.672	2021-12-31	0.8921	2022-08-29	-	2023-12-10	1.979
2020-08-28	4.981	2022-01-01	1.471	2022-09-11	6.202	2023-12-27	1.064
2020-09-19	3.478	2022-01-02	1.678	2022-09-17	8.115	2024-01-18	3.144
2020-10-24	17.58	2022-01-08	-	2022-09-25	3.985	2024-03-12	1.517
2020-10-25	3.868	2022-01-19	0.637	2022-09-30	4.66	2024-03-28	1.38
2020-11-18	-	2022-01-25	-	2022-10-01	-	2024-04-03	2.723
2020-11-19	-	2022-02-09	1.527	2022-10-19	9.037	2024-04-13	1.53
2020-12-25	9.832	2022-02-14	1.952	2022-11-06	4.528	2024-04-15	1.8
2021-01-10	15.61	2022-02-23	1.468	2022-11-11	8.102	2024-04-25	2.189
2021-01-31	-	2022-03-04	3.347	2022-11-27	32.41	2024-04-27	1.173
2021-04-03	20.24	2022-03-11	3.543	2022-12-24	12.62	2024-04-29	3.355
2021-05-12	1.994	2022-03-23	9.964	2023-01-16	3.693	2024-05-01	4.432
2021-05-14	3.438	2022-03-29	6.017	2023-02-05	6.608	2024-05-13	1.657
2021-05-22	7.754	2022-04-03	9.555	2023-02-13	-	2024-05-16	4.136
2021-09-03	-	2022-04-04	10.07	2023-02-16	3.927	2024-06-05	-
2021-09-18	-	2022-04-05	4.201	2023-03-02	3.674	2024-06-16	6.892
2021-10-09	-	2022-04-09	5.87	2023-04-01	0.3365	2024-07-17	18.23
2021-10-16	-	2022-04-12	7.715	2023-05-21	0.5204	2024-07-31	34.13
2021-10-21	-	2022-04-17	3.783	2023-05-25	0.653	2024-09-03	7.316
2021-11-13	1.641	2022-05-07	4.363	2023-05-26	0.4766	2024-10-26	3.198
2021-12-06	3.547	2022-05-08	3.543	2023-06-19	0.7229		

Notes.

^a The symbol – indicates that the noise diode was not injected for calibration on that observing day. The corresponding burst fluences are therefore unreliable and these data points are excluded from the correlation analysis.

Table 4. The S-band–converted PRS flux densities of FRB 20190520B

Date	Telescope	Flux density (μJy)	Date	Telescope	Flux density (μJy)
2020-07-21	VLA	198.9 \pm 12.3	2022-11-29	GMRT	196 \pm 32.2
2020-07-23	VLA	210.5 \pm 17.7	2022-12-27	GMRT	114 \pm 19
2020-08-17	VLA	182 \pm 12.6	2023-01-24	GMRT	205 \pm 30
2020-08-18	VLA	205.9 \pm 13.8	2023-02-21	GMRT	87 \pm 26.5
2020-08-29	VLA	198.3 \pm 11.3	2023-03-21	GMRT	205 \pm 18.3
2020-08-30	VLA	195 \pm 14	2023-06-07	VLA	157 \pm 9
2020-09-12	VLA	177 \pm 8.53	2023-06-15	VLA	173 \pm 11
2020-09-13	VLA	186 \pm 15	2023-06-17	VLA	171 \pm 12
2020-09-15	VLA	192 \pm 12.6	2023-06-18	VLA	166 \pm 7.4
2020-09-19	VLA	176 \pm 16	2023-06-20	VLA	147 \pm 4.76
2020-11-08	VLA	174.5 \pm 16.3	2023-06-23	VLA	147 \pm 13
2020-11-14	VLA	233 \pm 17	2023-06-24	VLA	148.7 \pm 9.8
2020-11-16	VLA	211 \pm 14	2024-08-08	VLA	170 \pm 10
2021-10-01	VLA	148 \pm 19.2	2024-09-03	VLA	168 \pm 17.5
2021-11-07	VLA	136 \pm 17.7	2024-09-12	VLA	134 \pm 11.7
2022-02-26	EVN	159 \pm 32.3	2024-09-21	VLA	139 \pm 14.6
2022-02-27	EVN	170 \pm 32.3			

Table 5. P_{day} Data of FRB 20240114A

Date	P_{day}^a	Date	P_{day}	Date	P_{day}	Date	P_{day}
2024-06-16	36.626	2024-07-21	173.398	2024-07-29	199.112	2024-08-15	125.8
2024-06-23	24.3684	2024-07-23	97.9424	2024-07-31	114.669	2024-08-18	82.8507
2024-06-30	21.6935	2024-07-25	89.4095	2024-08-03	121.384	2024-08-22	79.541
2024-07-07	32.7147	2024-07-27	148.509	2024-08-06	40.6069	2024-08-30	37.7285
2024-07-14	114.124	2024-07-28	140.522	2024-08-09	81.004		

Table 6. The S-band–converted PRS flux densities of FRB 20240114A

Date	Telescope	Flux density (μJy)	Date	Telescope	Flux density (μJy)
2024-06-15	GMRT	36.0 \pm 9.3	2024-07-28	GMRT	44.5 \pm 11.6
2024-07-03	GMRT	30.4 \pm 6.9	2024-07-29	VLA	84.8 \pm 6.9
2024-07-07	GMRT	37.4 \pm 11.6	2024-08-22	GMRT	42.0 \pm 9.2
2024-07-13	GMRT	53.9 \pm 14.4	2024-09-28	VLBA	54.7 \pm 10.7
2024-07-23	VLA	97.2 \pm 11.9	2024-09-30	VLBA	54.7 \pm 10.7
2024-07-27	VLA	79.5 \pm 6.5	2024-10-03	VLA	66.8 \pm 7.2



Figure 3. Permutation-test results for segment A of FRB 20190520B based on the ICCF analysis.

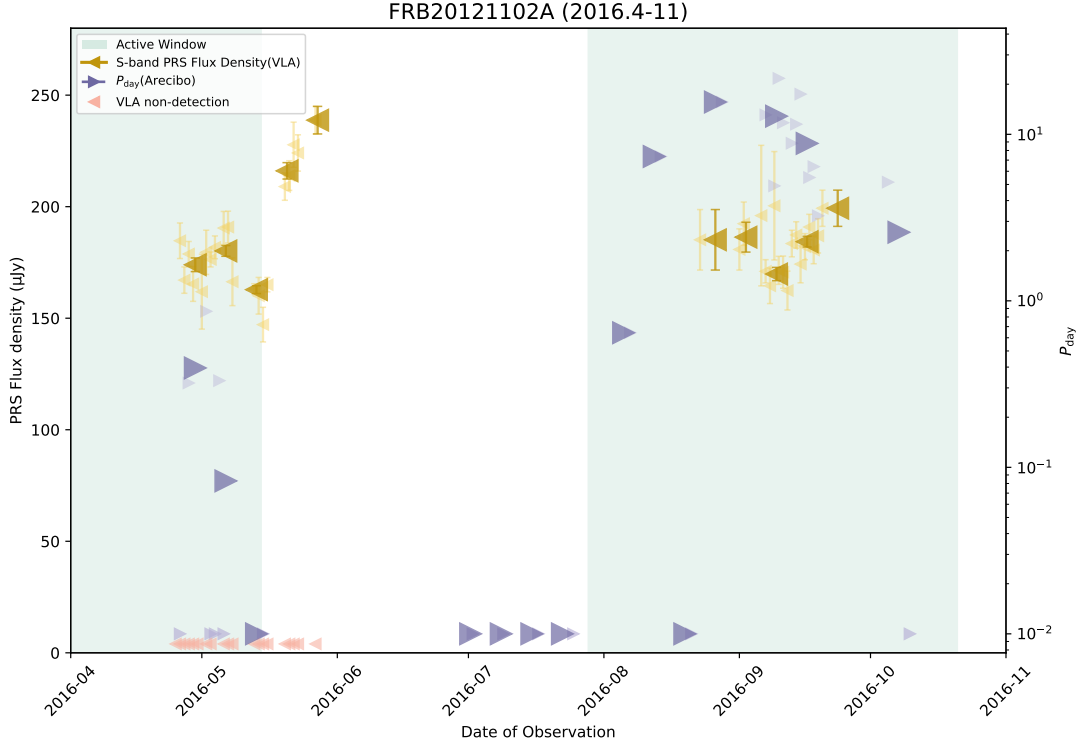


Figure 4. S-band PRS flux density of FRB 20121102A and the corresponding daily FRB activity proxy, P_{day} . The symbol definitions are the same as those used for FRB 20190520B. Unlike FRB 20190520B, however, the S-band PRS flux densities shown here are direct measurements and are not converted from other frequencies using a spectral index. The red markers along the bottom indicate VLA burst-search epochs in May 2016, during which no FRB bursts were detected. Given the limited number of data points and the relatively short temporal coverage, the binned values are computed using a 7-day binning scheme starting from the first PRS observation. Previous studies have shown that FRB 20121102A exhibits activity cycles in the L band, with a period of approximately 159 days (C. A. Braga et al. (2025); M. C. Espinoza-Dupouy et al. (2026)), of which about 84 days correspond to an active phase. The light-green shaded regions indicate the time intervals during which the source is expected to be in a relatively active state.

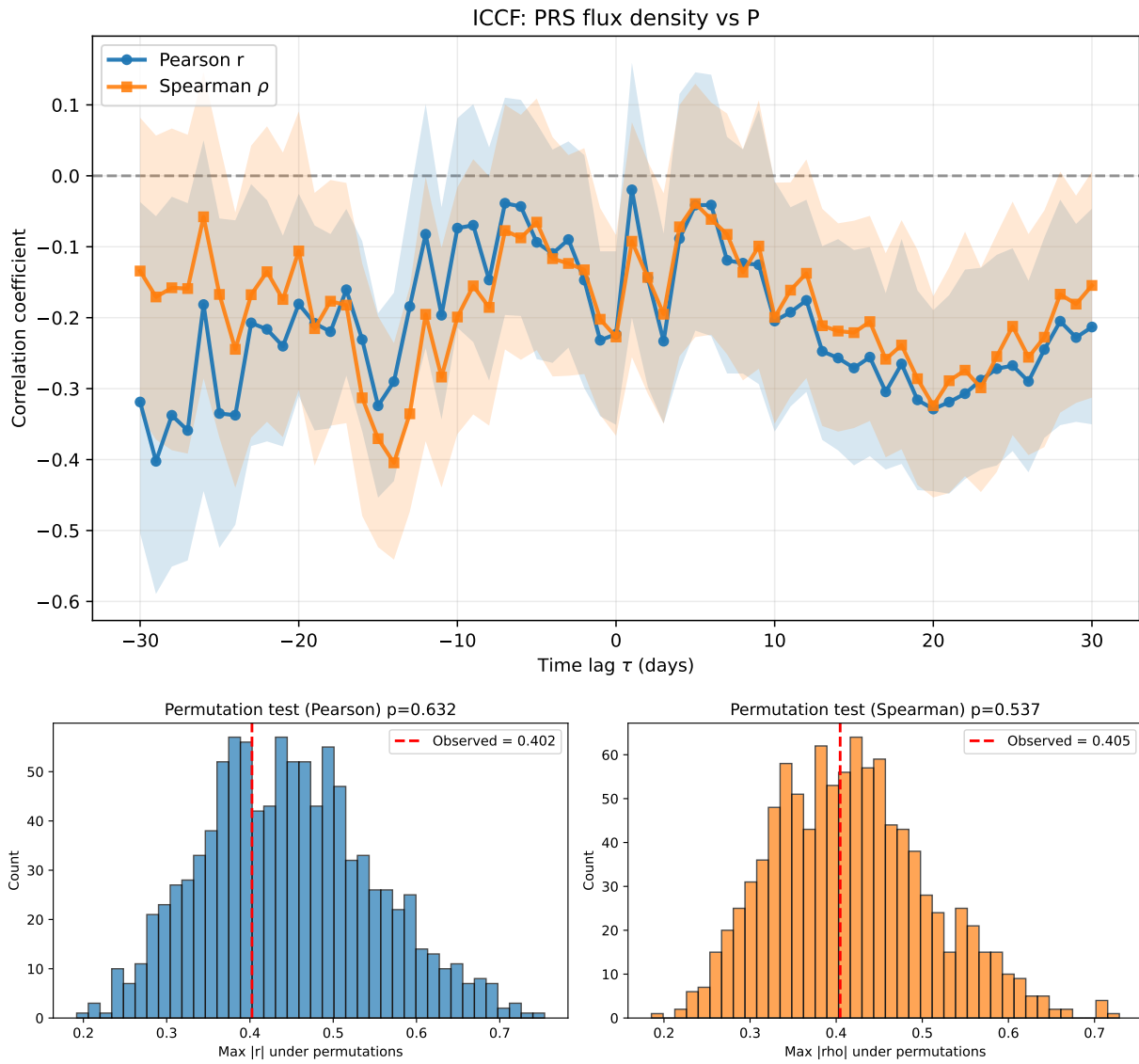


Figure 5. Permutation-test results for FRB 20121102A based on the ICCF analysis over the 2016 April–November interval.

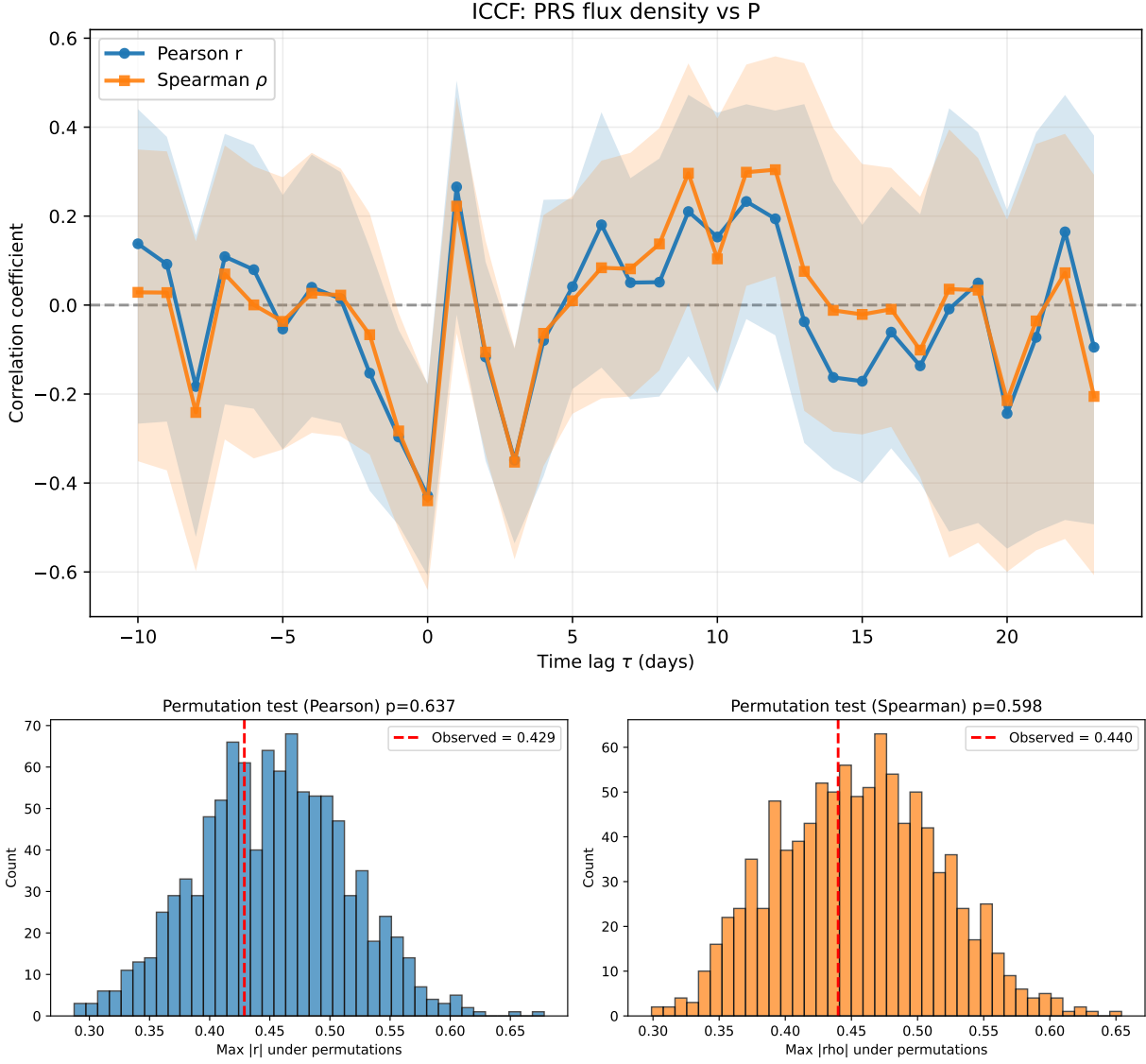


Figure 6. Permutation-test results for FRB 20121102A based on the ICCF analysis over the 2016 August–October sub-epoch. Correlation coefficients are reported only for lags where the number of valid paired points after interpolation exceeds the adopted minimum threshold; lags with insufficient effective pairs are left blank.

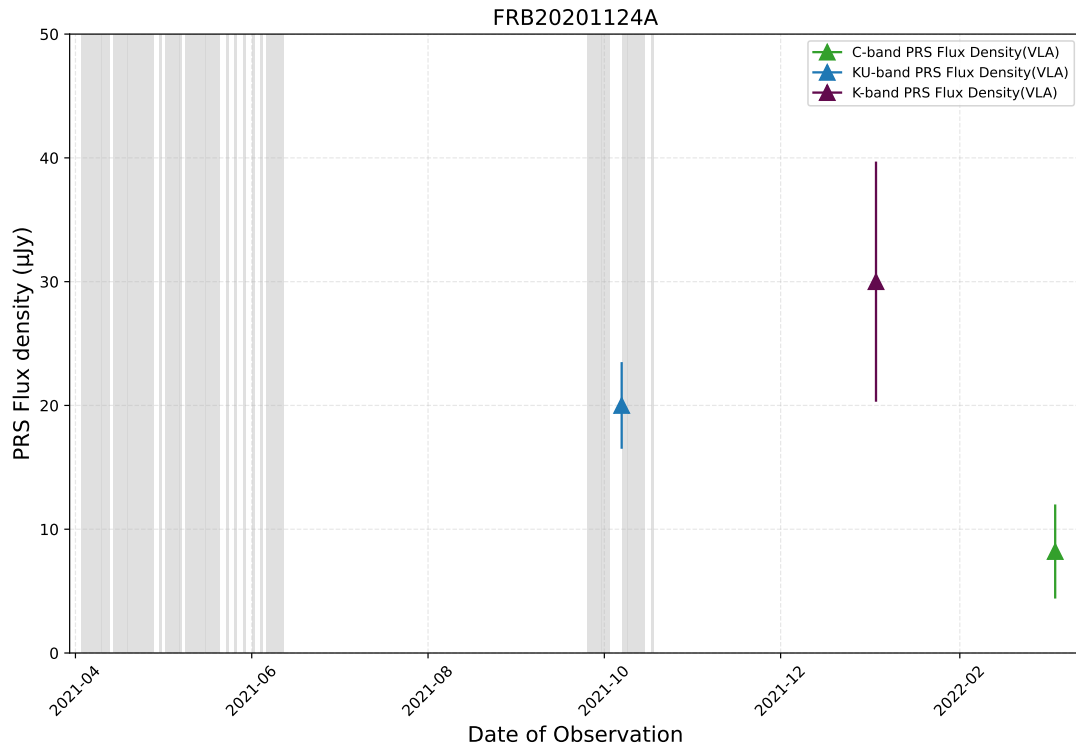


Figure 7. PRS flux-density measurements of FRB 20201124A, with gray shaded intervals indicating the epochs of FAST monitoring.